Relation between subduction megathrust earthquakes, trench sediment thickness and upper plate strain

Auxiliary Material

Authors: A. Heuret[1,2], C. P. Conrad[3], F. Funiciello[1], S. Lallemand[2], L. Sandri[4]

1 Dipartimento Scienze Geologiche, Università "Roma TRE", Rome, Italy

2 Géosciences Montpellier, CNRS, Montpellier 2 University, France

3 Dept. Geology & Geophysics, Univ. Hawaii at Manoa, Honolulu, Hawaii, USA

4 Istituto Nazionale di Geofisica e Vulcanologia, Sezione di Bologna, Italy

1. Database of sediment thickness at trench

We constrained sediment thickness at the trench (T_{sed}), and its lateral variability, for 44 trench sections (Figure 1) based on a compilation of published local seismic-reflection data from 160 sampled points (about 40% of the initial set of sampled points).

Previous compilations of trench sediment thickness (e.g., von Huene and Scholl, 1991; Lallemand et al., 1994; Clift and Vanucchi, 2004) have been generally based on only one seismic-reflection line per segment, often different from one compilation to the other. Because most trenches exhibit large and rapid along-strike variability in trench fill, this can lead to contradictory estimations between studies (e.g., the sediment thickness at the Manila trench is estimated at 1.5 km by von Huene and Scholl [1991] and at 4.5 km by Clift and Vannuchi [2004]).

The NOAA sediment thickness database [Divins] may constrain the T_{sed} lateral variability, but the database definition at trenches is generally too low. As a result, the sediment thicknesses measured in the NOAA database are, on average, underestimated by 1.0 ± 1.0 km relative to those measured using seismic-reflection data. Overestimated thicknesses account for only 26% of cases, and are 0.5 ± 1.1 km thicker on average.

The original dataset we provide here results from the compilation of published local seismic-reflection data (Figure 1), available for 160 of the initial set of sampled points (i.e., 40%). All the sampled points are listed, with their references, in Table 1. The resulting dataset (Table 2) not only provides estimates of T_{sed}, the mean trench sediment thickness for each of the 44 trench sections, but also some constraints on the lateral variability observed along each of these trench sections. For this, $T_{sed\ min}$ and $T_{sed\ max}$, the minimum and maximum trench sediment thicknesses observed along the trench section, are determined. Table 2 also provides, for each trench section, the number of points of the initial set of sampled points that are covered by seismic-reflection data. The coverage is heterogeneous from one trench section to another. Low coverage is without consequence where the sediment thickness is homogeneous laterally along the trench (e.g., Marianas, Tonga, S-Kuriles), but some trench sections exhibit rapid lateral changes in T_{sed}, sometimes varying several by kilometres within only several dozens kilometres along the trench (e.g., Manila, Colombia, New Britain). Such variations result from local conditions (e.g., vicinity of sediment supply, seamount collision with the trench, the presence of sediments traps) that can lead to T_{sed} misestimations where coverage is poor. Ws-Alaska, E-Aleutians, S-Kermadec, S-New Hebrides and N-New Hebrides trench sections have no referenced seismic reflection data but are constrained thanks to sampled points belonging to the adjacent transect.

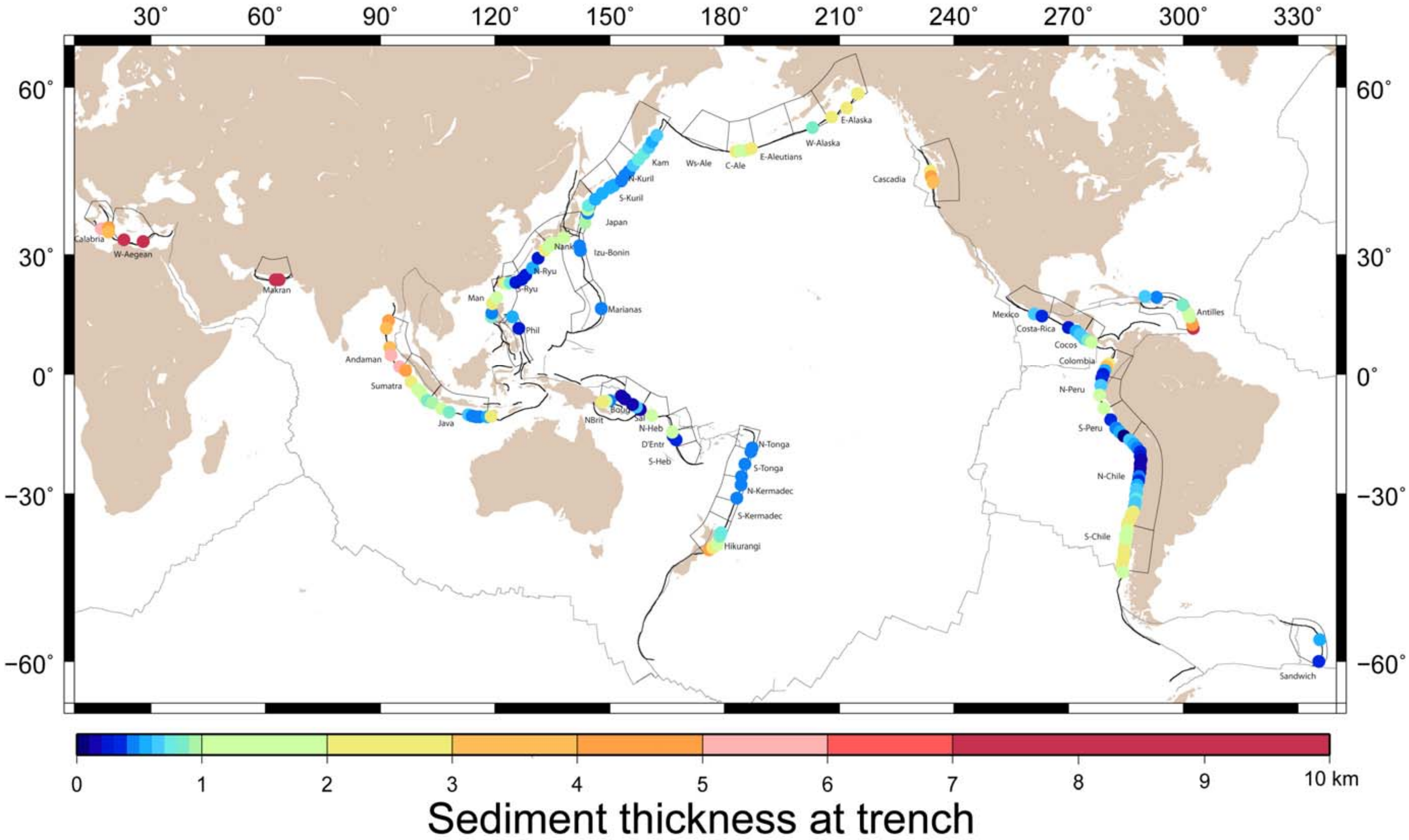

Figure S1: Map showing the location and T_{sed} values of the 160 sampled points.

Table S1: List of sampled points and associated references. (1) Chamot-Rooke et al. [2005]; (2) Reston et al. [2002]; (3) Kopp et al [2000]; (4) Moore et al. [1982]; (5) Dessa et al. [2009]; (6) Singh et al. [2008]; (7) Schlueter et al. [2002]; (8) Kopp et al. [2002]; (9) van der Werff [1995]; (10) Taylor and Hayes [1983]; (11) Lallemand et al. [1994]; (12) Bloomer and Fisher [1988]; (13) Font et al. [2001]; (14) Lallemand et al. [1999]; (15) Letouzey and Kimura [1985]; (16) Park et al. [1998]; (17) Park et al. [2002]; (18) Lallemand et al. [1992]; (19) Mrozowski et al. [1982]; (20) Taylor [1992]; (21) von Huene [1986]; (22) Klaeschen et al. [1994]; (23) Gnibidenko et al. [1983]; (24) McCarthy and Scholl [1985]; (25) Ryan and Scholl [1989]; (26) von Huene and Klaeschen [1999]; (27) Brocher et al. [1994]; (28) Fuis et al. [2008]; (29) Shipley and Moore [1985]; (30) Ranero et al. [2000]; (31) Hinz et al. [1996]; (32) Collot et al. [2004]; (33) Sage et al. [2006]; (34) Calahoranno [2005] ; (35) Kukowski et al. [1994]; (36) Hoffmann-Rothe et al. [2006]; (37) Westbrook et al. [1988]; (38) Masson and Scanlon [1991]; (39) Vanneste et al. [2002]; (40) Vanneste and Larter [2002]; (41) Lewis et al. [1998] ; (42) Barker et al. [2009]; (43) Furumoto et al. [1970]; (43) Mann and Taira [2004]; (45) Bruns et al. [1989]; (46) Galewsky and Silver [1997].

Trench section	Longitude (°N)	Latitude (°W)	T_{sed} (km)	Reference
Calabria	17.0	35.7	5.0	1
W-Aegean	18.9	36	4.5	1
W-Aegean	18.9	35	3.5	2
W-Aegean	23.0	33.3	7.0	1
W-Aegean	28.0	33.0	10.0	1
Makran	62.5	24.1	7.6	3
Makran	63.5	24.1	7.6	3
Andaman	92.1	14.0	4.5	4
Andaman	91.6	12.0	3.0	4
Andaman	92.5	7.0	3.5	4
Andaman	92.8	5.0	5.0	4
Andaman	95	2.0	5.0	5
Sumatra	96.6	1.0	4.0	4
Sumatra	98.1	-2.0	2.2	4
Sumatra	99.7	-4.0	1.5	4
Sumatra	100.5	-4.7	1.0	4
Sumatra	101.5	-6.2	1.0	6
Sumatra	102.3	-7.0	0.9	7
Java	103.7	-7.7	0.9	7
Java	106.0	-9.1	1.5	8
Java	108.0	-10	0.8	4
Java	113.0	-10.7	0.6	4
Java	114.0	-11	0.4	9
Java	115.0	-11.2	0.4	9
Java	116.0	-11.2	0.4	9
Manila	119.1	15.0	0.8	10
Manila	119.2	16.0	0.4	10
Manila	119.3	18.3	2.5	10
Manila	120.4	19.7	1.5	11
Philippines	126.2	12.0	0.2	12

Philippines	124.5	15.0	0.5	12
S-Ryukyu	122.5	23.3	2.5	13
S-Ryukyu	123.2	23.2	1.8	14
S-Ryukyu	124.0	23.4	0.8	15
S-Ryukyu	125.5	23.5	0.2	16
N-Ryukyu	127.0	24.2	0.2	16
N-Ryukyu	128.0	25.2	0.3	15
N-Ryukyu	129.8	26.9	0.5	15
N-Ryukyu	131.3	29.2	0.2	15
Nankai	133.0	31.1	2.3	17
Nankai	134.0	31.8	1.7	11
Nankai	134.7	32.6	1.2	17
Nankai	135.5	32.6	1.5	17
Nankai	138.0	33.8	1.5	18
Marianas	147.8	17.0	0.4	19
Izu-Bonin	142.3	31.0	0.4	20
Izu-Bonin	142.1	32.0	0.4	20
Japan	143.5	37.0	0.9	11
Japan	144.2	39.0	0.4	11
Japan	144.2	39.7	1.2	21
Japan	144.5	40.5	0.7	11
S-Kuriles	146.2	41.8	0.5	11
S-Kuriles	148.0	42.9	0.5	22
S-Kuriles	150.0	44.0	0.5	23
S-Kuriles	151.0	44.4	0.5	23
N-Kuriles	153.0	45.3	0.4	23
N-Kuriles	154.0	46.2	0.4	22
N-Kuriles	155.1	47.0	0.4	23
N-Kuriles	156.2	48.0	0.6	23
N-Kuriles	157.5	49.0	0.7	22
Kamchatka	159.0	50.0	0.8	23
Kamchatka	160.2	51.0	0.6	23
Kamchatka	161.1	52.0	0.5	23
Kamchatka	162.3	53.0	0.6	23
C-Aleutians	183.0	50.4	2.0	24
C-Aleutians	184.0	50.5	1.8	25
C-Aleutians	185.0	50.5	1.2	21
C-Aleutians	186.0	50.7	1.0	25
C-Aleutians	187.0	50.9	2.0	25
W-Alaska	203.0	54.2	0.8	21
E-Alaska	208.0	55.8	2.8	21
E-Alaska	212.0	57.1	2.7	26
E-Alaska	214.7	59.1	2.8	27
E-Alaska	215.0	59.1	2.5	28
Cascadia	233.9	47.0	2.0	11

Cascadia	234.1	46.0	4.1	21
Cascadia	234.5	45.0	3.7	21
Mexico	261.0	15.8	0.6	21
Mexico	263.0	15.2	0.3	29
Costa-Rica	270.0	12.3	0.2	29
Costa-Rica	272.0	11.4	0.5	30
Costa-Rica	273.0	10.5	0.6	11
Cocos	274.0	9.4	0.6	21
Cocos	275.0	8.9	0.8	31
Cocos	276.0	8.4	1.5	31
Colombia	280.5	2.8	2.0	32
Colombia	279.9	2.0	3.0	32
Colombia	279.5	1.0	0.5	32
Colombia	279.0	0.0	0.2	32
N-Peru	278.7	-1.0	0.3	33
N-Peru	278.5	-3.0	0.6	34
N-Peru	278.1	-5.5	1.5	21
N-Peru	279.2	-9.0	1.0	21
S-Peru	281.0	-12.0	0.3	35
S-Peru	282.4	-14.0	0.4	36
S-Peru	283.4	-15.0	0.5	36
S-Peru	284.5	-16.0	0.1	36
N-Chile	285.9	-17.0	0.6	36
N-Chile	287.1	-18.0	0.5	36
N-Chile	288.0	-19.0	0.4	36
N-Chile	288.7	-20.0	0.3	36
N-Chile	288.7	-21.0	0.2	36
N-Chile	288.9	-22.0	0.1	36
N-Chile	288.7	-23.0	0.1	36
N-Chile	288.7	-24.0	0.1	36
N-Chile	288.6	-25.0	0.1	36
N-Chile	288.4	-26.0	0.4	36
N-Chile	288.3	-27.0	0.3	36
N-Chile	288.0	-28.0	0.5	36
N-Chile	287.7	-29.0	0.6	36
N-Chile	287.7	-29.7	0.6	36
N-Chile	287.5	-30.5	0.6	36
N-Chile	287.6	-31.2	0.7	36
N-Chile	287.4	-32.0	0.6	36
N-Chile	287.2	-33.0	0.6	36
N-Chile	286.9	-34.0	2.4	36
N-Chile	286.4	-34.7	2.4	36
N-Chile	286.2	-35.5	2.4	36
N-Chile	285.6	-36.2	2.3	36
S-Chile	285.4	-37.0	2.3	36

S-Chile	285.4	-38.0	1.5	36
S-Chile	284.9	-39.0	1.5	36
S-Chile	284.9	-40.0	1.5	36
S-Chile	284.7	-41.0	1.5	36
S-Chile	284.5	-42.0	2.0	36
S-Chile	284.5	-43.0	2.0	36
S-Chile	284.2	-44.0	2.0	36
S-Chile	283.9	-45.0	2.3	36
Antilles	302.6	12.0	8.0	11
Antilles	302.4	13.0	4.5	11
Antilles	301.7	15.0	1.0	11
Antilles	301.2	16.0	1.0	37
Antilles	299.8	18.0	0.8	11
Antilles	293.0	19.8	0.4	38
Antilles	290.0	20.0	0.6	38
Sandwich	335.4	-60.0	0.3	39
Sandwich	335.7	-57.0	0.5	40
Hikurangi	176.0	-41.8	4.2	41
Hikurangi	177.0	-41.4	2.8	42
Hikurangi	178.2	-40.7	1.7	11
Hikurangi	178.8	-39.2	0.8	42
Hikurangi	179.1	-38.5	0.8	42
N-Kermadec	183.2	-31.0	0.4	11
N-Kermadec	184.3	-28.0	0.4	11
S-Tonga	184.5	-26.0	0.4	11
S-Tonga	185.4	-23.0	0.4	11
S-Tonga	186.9	-20.0	0.4	11
N-Tonga	187.2	-19.0	0.4	11
D'Entrecasteaux	167.4	-17.0	0.3	21
D'Entrecasteaux	166.6	-16.0	0.3	11
D'Entrecasteaux	166.3	-15.0	1.2	21
Salomons	161.0	-10.9	1.3	43
Salomons	158.0	-9.3	0.1	44
Bougainville	157.0	-8.6	0.6	43
Bougainville	156.0	-8.0	0.1	45
Bougainville	154.0	-6.5	0.1	43
New Britain	153.0	-5.8	0.1	43
New Britain	150.0	-7.0	0.4	46
New Britain	149.0	-7.1	1.1	46
New Britain	148.0	-7.3	2.5	46

Table S2: T_{sed}, $T_{sed\ min}$, $T_{sed\ max}$, the number of samples covered by observations (N_{obs}), the number of sample points in the initial set (N_{tot}), *UPS*, and M_{max}, for the 44 trench segments.

Segment	T_{sed}	$T_{sed\ min}$	$T_{sed\ max}$	N_{obs}	N_{tot}	*UPS*	M_{max}
Calabria	5.0	5.0	5.0	1	6	E	7.0
W-Aegean	6.3	3.5	10.0	4	17	E	7.8
Makran	7.6	7.6	7.6	2	9	N	8.0
Andaman	4.2	3.0	5.5	5	13	N	9.0
Sumatra	1.8	0.9	4.0	6	10	N	8.8
Java	0.7	0.4	1.5	7	14	N	7.8
Manila	1.3	0.4	2.5	4	13	C	7.5
Philippines	0.4	0.2	0.5	2	13	C	7.7
S-Ryukyu	1.3	0.2	2.5	4	4	E	7.9
N-Ryukyu	0.3	0.2	0.5	4	8	E	7.7
Nankai	1.6	1.2	2.3	5	11	N	8.6
Marianas	0.4	0.4	0.4	1	17	E	7.5
Izu-Bonin	0.4	0.4	0.4	2	11	E	7.9
Japan	0.8	0.4	1.2	4	9	C	9.1
S-Kuriles	0.5	0.5	0.5	4	7	N	8.6
N-Kuriles	0.5	0.4	0.6	4	4	N	8.3
Kamchatka	0.6	0.5	0.8	5	7	N	9.0
Ws-Aleutians	1.3	1.0	2.0	0	11	N	8.7
C-Aleutians	1.6	1.0	2.0	5	7	N	8.6
E-Aleutians	1.4	0.8	2.0	0	10	N	8.0
W-Alaska	0.8	0.8	0.8	1	9	N	8.0
E-Alaska	2.7	2.7	2.8	4	13	N	9.2
Cascadia	3.3	2.0	4.1	3	9	N	9.0
Mexico	0.5	0.3	0.6	2	11	N	8.0
Costa-Rica	0.4	0.2	0.6	3	9	N	7.7
Cocos	1.0	0.6	1.5	3	3	C	7.4
Colombia	1.4	0.2	3.5	4	7	C	8.6
N-Peru	0.9	0.3	1.5	4	10	C	7.8
S-Peru	0.3	0.1	0.5	4	7	C	8.2
N-Chile	0.8	0.1	2.3	22	22	C	8.8
S-Chile	1.8	1.5	2.4	9	9	N	9.5
Antilles	2.3	0.4	8.0	7	17	N	8.3
Sandwich	0.4	0.3	0.5	2	11	E	7.2
Hikurangi	2.1	0.8	4.2	5	9	N	7.7
S-Kermadec	0.4	0.4	0.4	0	4	E	6.6
N-Kermadec	0.4	0.4	0.4	2	6	E	8.0
S-Tonga	0.4	0.4	0.4	2	6	E	8.0
N-Tonga	0.4	0.4	0.4	2	6	E	8.0
S-NewHebrides	0.3	0.3	1.2	0	6	E	7.9
Dentrecasteaux	0.6	0.3	1.2	2	3	N	7.6
N-NewHebrides	0.3	0.3	1.2	1	4	E	7.7
Salomons	0.7	0.1	1.3	2	7	N	7.9
Bougainville	0.3	0.1	0.6	3	4	N	8.1
NewBritain	1.0	0.1	2.5	4	6	E	8.1

2. Simulation of synthetic datasets

In order to quantify the probability of observing the patterns shown in Figure 3 by chance, we run different sets of Monte Carlo simulations. First, we distinguish 4 classes of M_{max}:

- Class 1: $M_{max} < 8.0$.
- Class 2: $8.0 \leq M_{max} < 8.5$.
- Class 3: $8.5 \leq M_{max} < 9.0$.
- Class 4: $M_{max} \geq 9.0$.

Next, we investigate the individual and combined roles of T_{sed} and *UPS*. When investigating the role of T_{sed}, we consider the following conditions:

- $T_{sed} < 0.5$ km.
- $0.5 \leq T_{sed} < 1.0$ km.
- $T_{sed} \geq 1.0$ km.

When investigating the role of *UPS*, we consider the following conditions:

- Extensional *UPS*.
- Compressive *UPS*.
- Neutral *UPS*.

When considering the combined role of T_{sed} and *UPS*, we divide the domain [T_{sed}; *UPS*] into 3 specific Field types (as in Figure 3):

-Field 1: Extensional *UPS* or $T_{sed} < 0.5$ km

-Field 2: Compressive *UPS* and $T_{sed} \geq 0.5$ km, or Neutral *UPS* and $0.5 \leq T_{sed} < 1.0$ km

-Field 3: Neutral *UPS* and $T_{sed} \geq 1.0$ km

We generate 10,000 synthetic datasets, each consisting of 44 randomly selected T_{sed} and *UPS* values attached to each of the M_{max} values observed. In each synthetic catalog, the 44 *UPS* types are a random permutation of the 44 actual values of *UPS* (so that there are 22 N-type, 8 C-type and 14 E-type synthetic subduction zones), while the 44 T_{sed} values are sampled from T_{sed} empirical cumulative distribution between 0 and 10 km (see Figure S2). Hence, about 80% of the synthetic subduction zones have $T_{sed} \leq 2$ km, reproducing the observed distribution apparent for Earth's current subduction zones.

For each synthetic catalog, we count how many simulated subduction zones of the different M_{max} classes fall under the three defined conditions, and we build up frequency histograms (see Figures S3 to S5). For every class and conditions, we test two different null hypotheses. The first is $H_{0\text{-}1}$: $N_{real} \leq N_{synth}$ (opposite to the alternative hypothesis $H_{1\text{-}1}$: $N_{real} > N_{synth}$); to test this hypothesis, we count how many of the 10,000 synthetic catalogs have a number of subduction zones (N_{synth}) equal to or larger than the actual observed number (N_{real}). We divide that number, which we compute for every combination of M_{max} and condition (T_{sed}, *UPS*, or field), by 10,000 to we obtain a p-value (top value in panels in Figures S3 to S5). The second null hypothesis we test is $H_{0\text{-}2}$: $N_{real} \geq N_{synth}$ (alternative hypothesis is $H_{1\text{-}2}$: $N_{real} < N_{synth}$), and here we count how many of the 10,000 synthetic catalogs have an N_{synth} equal to or smaller than the actual N_{real}. We again obtain p-values for every class and condition (bottom value in panels in Figures S3 to S5) by dividing that number by 10,000. These two p-values represent the probability that a synthetic catalog may have by chance a number of trenches for a specific class and condition that is equal to or larger/smaller (respectively for the two null hypotheses) than the observed number in the real catalog. In particular, low (< 5%) p-values mean that the observed number of real trenches is significantly (at the 5% significance level) higher/smaller than would be expected by pure chance.

From Figure S3, we see that GEQs ($M_{max} \geq 8.5$) tend not to occur in trench sections with $T_{sed} < 0.5$ km (but the bottom p-value is only < 5% for M_{max} between 8.5 and 8.9).

From Figure S4, we see that trenches with $M_{max} < 8.0$ are *(i)* more frequent where *UPS* is extensional (top p-value < 5%), and *(ii)* rarer where *UPS* is neutral (bottom p-value smaller than 1%), compared to expectations by random chance.

From Figure S5, we see that performing our statistical analysis using both T_{sed} and *UPS* parameters together provides additional information about the M_{max} distribution compared to what is learned when considering T_{sed} or *UPS* alone. In particular, besides obtaining similar results on the relatively rare occurrence of $M_{max} < 8.0$ in Field 3 (but not at the 5% level) and of GEQs in Field 1 (bottom p-values <1%), we also find that GEQs occur preferentially in Field 3 (p-values for $8.5 < M_{max} < 8.9$ and for $8.5 \geq 9.0$ in such regions are < 5%).

In order to check the stability of these patterns, we repeated the simulations by sampling from uniform distributions for *UPS* and T_{sed} (i.e., the 3 *UPS* types have the same probability of being sampled, and analogously T_{sed} is sampled from a uniform distribution between 0 and 10 km). Even though this test might produce biased p-values, as the proportion of the simulated subduction zones in the different conditions is not similar to reality, the patterns found are comparable to the one shown above.

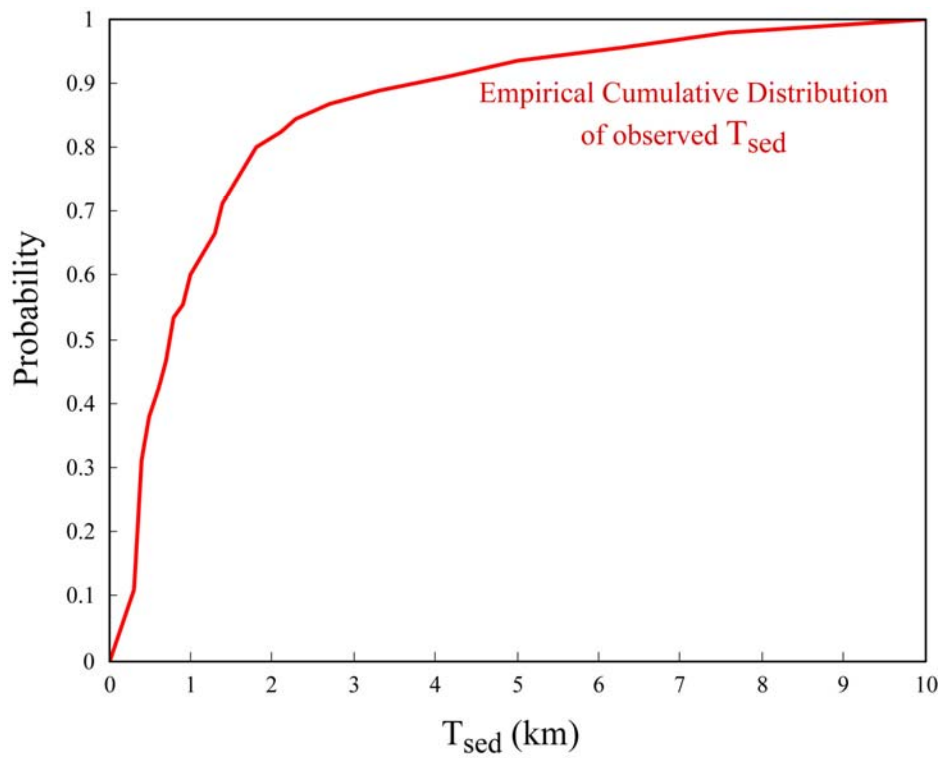

Figure S2: Empirical cumulative distribution used to sample T_{sed}. In the range between the minimum and maximum values of T_{sed} observed in the real catalog, the points of the empirical cumulative distribution show the number of real subduction zones with a T_{sed} smaller than or equal to the values on the x-axis, divided by the total number of subduction zones (i.e., 44). We extend, on the x-axis, the possible range of T_{sed} below the minimum T_{sed} and above the maximum value by connecting, respectively, these extremes to the points (T_{sed}= 0 km, y=0) and (T_{sed}=10 km, y=1).

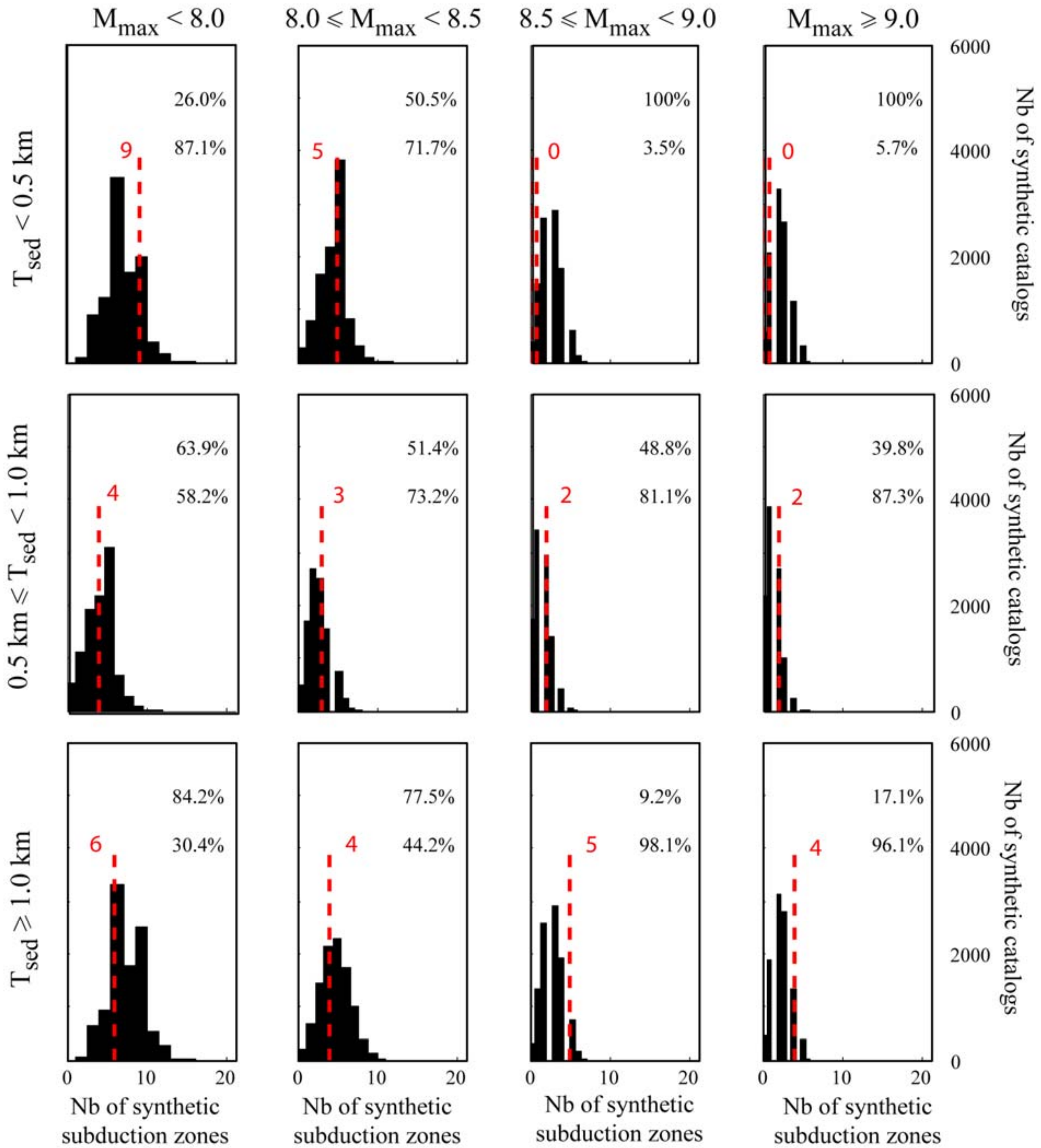

Figure S3: Histograms of the number of synthetic subduction zones for different conditions on the T_{sed} domain (along rows) and for different classes of M_{max} (along columns). In each panel, the red dashed line and number show the observed number of subduction zones in the real catalog for that T_{sed} condition and M_{max} class. The relative p-values for that T_{sed} condition and M_{max} class are given by the top number (probability of observing a synthetic number of subduction zones larger than or equal to the real one) and the bottom number (probability of observing a synthetic number of subduction zones smaller than or equal to the real one).

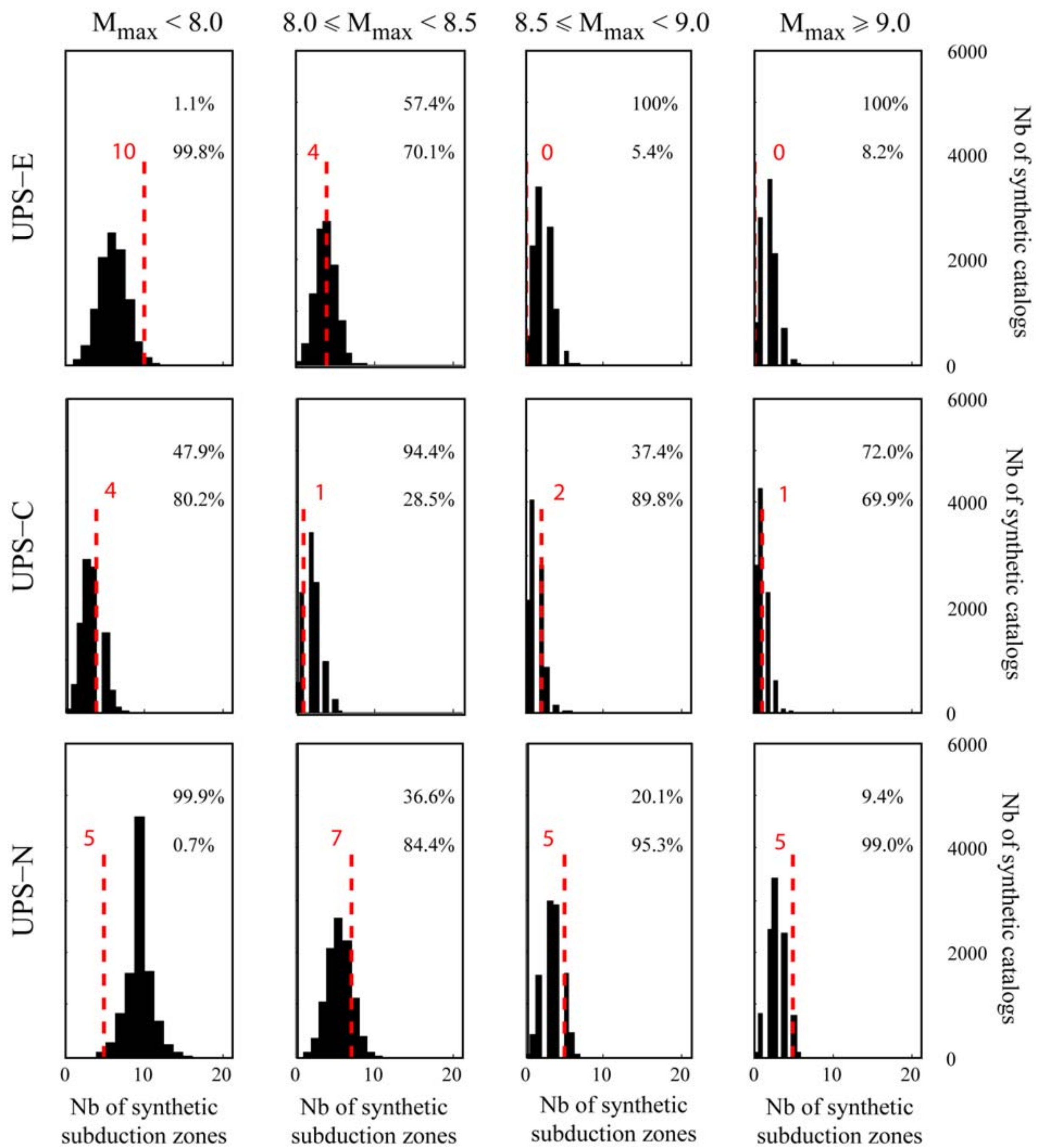

Figure S4: Similar to Figure S3, but showing histograms of the number of synthetic subduction zones for different conditions on the *UPS* domain (along rows) and different classes of M_{max} (along columns). The observed number of subduction zones and the computed p-values are as in Figure S3.

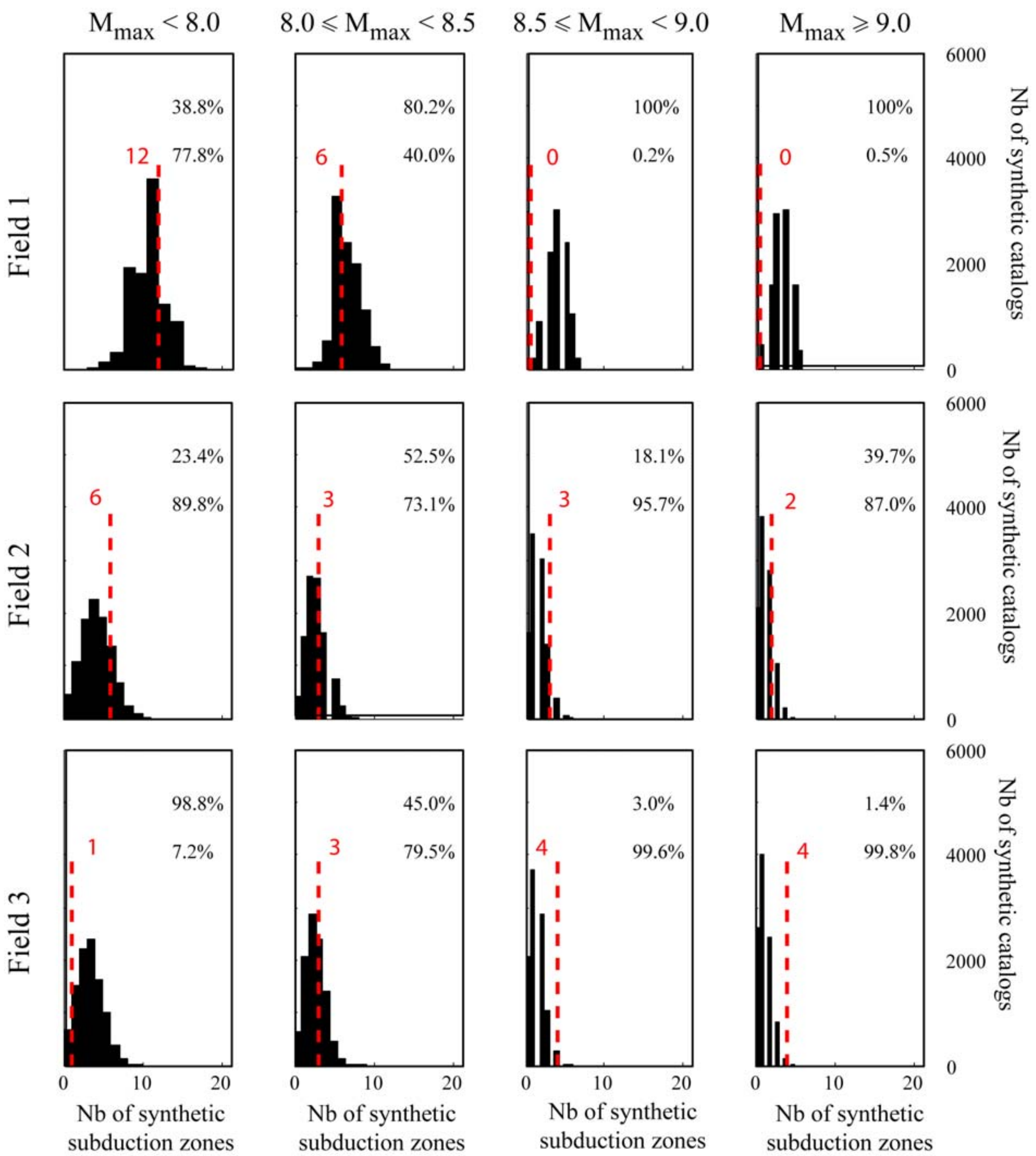

Figure S5: Similar to Figure S3, but showing histograms of the number of synthetic subduction zones for different fields of the [T_{sed}; UPS] domain (along rows) and different classes of M_{max} (along columns). The observed number of subduction zones and the computed p-values are as in Figure S3.

References:

Barker D.H.N., R. Sutherland, S. Henrys, S. Bannister (2009), Geometry of the Hikurangi subduction thrust and upper plate, North Island, New Zealand, *Geochem. Geophys. Geosys.*, 10 (2), Q02007, doi:10.1029/2008GC002153.

Bloomer S.H., R.L. Fisher (1988), Arc volcanic rocks characterize the landward slope of the Philippine Trench off northeastern Mindanao, *J. Geophys. Res.*, 93 (B10), 11961-11973.

Brocher T.M., G.S. Fuis, M.A. Fisher, G. Plafker, M. J. Moses, J.J. Taber, N.I. Christensen (1994), Mapping the megathrust beneath the northern Gulf of Alaska using wide-angle seismic data, *J. Geophys. Res.*, 99 (B6), 11663–11685.

Bruns T.R., J.G. Vedder, A.K. Cooper (1989), Geology of the Shortland Basin Region, Central Solomons Through, Solomon Islands - Review and new findings, in: Geology and offshore resources of Pacific island arc, mo Islands and Bougainville, Papua New Guinea Regions: Houston, Texas, Circum-Pacific Council for Energy and Mineral Resources Earth Science Series, 12, Eds: Vedder J.G. and T.R. Bruns.

Calahorrano A.B. (2005), Structure de la marge du golfe de Guayaquil (Equateur) et propriétés physiques du chenal de subduction à partir de données de sismique marine réflexion et réfraction, Thèse de l'Université Pierre et Marie Curie, Paris VI.

Chamot-Rooke N., C. Rangin, X. Le Pichon, A. Rabaute, O. Laurent, F. Ego, S. Lallemant, C. Nielsen, P. Pagot, D. Tsang Hin Sun, R. Walcott, R. Bousquet (2005), DOTMED, Deep Offshore Tectonics of the Mediterranean, A synthesis of deep marine data in the Eastern Mediterranean, Mémoire de la Société Géologique de France, n.s., 177, pp 64.

Collot J.-Y., B. Marcaillou, F. Sage, F. Michaud, W. Agudelo, P. Charvis, D. Graindorge, M.-A. Gutscher, and G. Spence (2004), Are rupture zone limits of great subduction earthquakes controlled by upper plate structures? Evidence from multichannel seismic reflection data acquired across the northern Ecuador– southwest Colombia margin, *J. Geophys. Res.*, 109 (B11103), doi:10.1029/2004JB003060.

Dessa J.-X., F. Klingelhoefer, D. Graindorge, C. André, H. Permana, M.-A. Gutscher, A. Chauhan, S.C. Singh and the SUMATRA-OBS Scientific Team (2009), Megathrust earthquakes can nucleate in the forearc mantle: evidence from the 2004 Sumatra event, *Geology*, 37 (7), 659-662, doi: 10.1130/G25653A.1.

Divins D.L., NGDC Total Sediment Thickness of the World's Oceans & Marginal Seas database (http://www.ngdc.noaa.gov/mgg/sedthick/sedthick.html.

Font Y., C.-S. Liu, P. Schnürle, S. Lallemand (2001), Constraints on backstop geometry of the Southwest Ryukyu subduction based on reflection seismic data, *Tectonophysics*, 333 (1-2), 135-158.

Fuis G.S., T.E. Moore, G. Plafker, T.M. Brocher, M.A. Fisher, W.D. Mooney, W.J. Nokleberg, R.A. Page, B.C. Beaudoin, N.I. Christensen, A.R. Levander, W.J. Lutter, R.W. Saltus, N.A. Ruppert (2008), Trans-Alaska Crustal Transect and continental evolution involving subduction underplating and synchronous foreland thrusting, *Geology*, 36 (3), 267-270.

Furumoto A.S., D.M. Hussong, J.F. Campbell, G.H. Sutton, A. Malahoff, J.C. Rose, G.P. Woollard (1970), Crustal and Upper Mantle Structure of the Solomon Islands as Revealed by Seismic Refraction Survey of November-December 19661, *Pacific Science*, 24, 315-322.

Galewsky J. and E.A. Silver (1997), Tectonic controls on facies transitions in an oblique collision: The western Solomon Sea, Papua New Guinea, *GSA Bull.*, 109 (10), 1266-1278.

Gnibidenko H., T.G. Bykova, O.V. Vorobiev, A.S. Svarichevsky (1983), The tectonics of the Kuril-Kamchatka deep-sea trench, in: Geodynamics of the Western Pacific-Indonesian Region, *Geodyn. Ser.*, 11, 249-285, Eds: Hilde T.W.C. and S. Uyeda, doi:10.1029/GD011p0249.

Hinz K., R. von Huene, C.R. Ranero (1996), Tectonic structure of tje convergent Pacific margin offshore Costa-Rica from multichannel seismic reflection data, *Tectonics*, 15 (1), 54-66.

Hoffmann-Rothe A., N. Kukowski, G. Dresen, H. Echtler, O. Oncken, J. Klotz, E. Scheuber, A. Kellner (2006), Oblique convergence along the Chilean margin: partitionning, margin parallel faulting and forces interaction at the plate interface, in: The Andes - Active subduction orogeny - Springer, Eds: O. Oncken, 551-581.

Klaeschen D., I. Belykh, H. Gnibidenko, S. Patrikeyev, R. von Huene (1994), Structure of the Kuril Trench from seismic reflection records, *J. Geophys. Res.*, 99 (B12), 24173-24188.

Kopp C., J. Fruehn, E.R. Flueh, C. Reichert, N. Kukowski, J. Bialas, D. Klaeschen (2000), Structure of the Makran subduction zone from wide-angle and reflection seismic data, *Tectonophysics*, 329, 171-191.

Kopp H., D. Klaeschen, E.R. Flueh, J. Bialas (2002), Crustal structure of the Java margin from seismic wide-angle and multichannel reflection data, *J. Geophys. Res.*, 107 (B2), 2034, doi:10.1029/2000JB000095.

Kukowski N., R. von Huene, J. Malavieille, S. Lallemand (1994), Sediment accretion against a buttress beneath the Peruvian continental margin at 12 degrees S as simulated with sandbox modeling, *Geol. Rundsch.*, 83 (4), 822-831.

Lallemand S., J. Malavieille, S. Calassou (1992), Effects of oceanic ridge subduction on accretionary wedges; experimental modeling and marine observations, *Tectonics*, 11 (6), 1301-1313.

Lallemand S., P. Schnürle, J. Malavieille (1994), Coulomb theory applied to accretionary and nonaccretionary wedges: possible causes for tectonic erosion and/or frontal accretion, *J. Geophys. Res.,* 99 (B6), 12033-12055.

Lallemand S., C.-S. Liu, S. Dominguez, P. Schnürle, J. Malavieille (1999), Trench-parallel stretching and folding of forearc basins and lateral migration of the accretionary wedge in the southern Ryukyus: a case of strain partition caused by oblique convergence, *Tectonics*, 18 (2), 231-247.

Letouzey J. and M. Kimura (1985), Okinawa Trough genesis: structure and evolution of a backarc basin developed in a continent, *Marine and Petroleum Geology*, 2, 111-130.

McCarthy J. and D.W. Scholl (1985), Mechanism of subduction accretion along the central Aleutian Trench, *GSA Bull.*, 96, 691-701.

Lewis K.B., J.Y. Collot, S. Lallemand (1998), The damned Hikurangi Trough; a channel-fed trench blocked by subducting seamounts and their wake avalanches (New Zealand – France GeodyNZ Project), *Basin Res.*, 10 (4), 441-468.

Masson D.G. and K.M. Scanlon (1991), The neotectonic setting of Puerto Rico, *GSA Bull.*, 103 (1), 144-154.

Mann P. and A. Taira (2004), Global tectonic significance of the Solomon Islands and Ontong Java Plateau convergent zone, *Tectonophysics*, 389 (3-4), 137-190, Eds: Mann P. and A. Taira.

Moore G.F., J.R. Curray, F.J. Emmel (1982), Sedimentation in the Sunda Trench and forearc region, Special Publication - *Geological Society of London*, 10, 245-258, Eds: J.K. Leggett.

Mrozowski C.L., D.E. Hayes, B. Taylor (1982), Multichannel Seismic Reflection Surveys of Leg 60 Sites, Deep Sea Drilling Project, doi:10.2973dsdp.proc.60.104.1982.

Park J.-O., H. Tokuyama, M. Shinohara, K. Suyehiro, A. Taira (1998), Seismic record of tectonic evolution and backarc rifting in the southern Ryukyu island arc system, *Tectonophysics*, 294 (1-2), 21-42.

Park J.-O., T. Tsuru, N. Takahashi, T. Hori, S. Kodaira, A. Nakanishi, S. Miura, Y. Kaneda (2002), A deep strong reflector in the Nankai accretionary wedge from multichannel seismic data; implications for underplating and interseismic shear stress release, *J. Geophys. Res.*, 107 (B4), doi: 10.1029/2001JB000262.

Ranero C.R., R. von Huene, E. Flueh, M. Duarte, D. Baca, K. McIntosh (2000), A cross section of the convergent Pacific margin of Nicaragua, *Tectonics*, 19 (2), 335-357.

Reston T.J., J. Fruehn, R. von Huene, IMERSE Working Group (2002), The structure and evolution of the western Mediterranean Ridge, *Marine Geology*, 186, 1-2, 83-110, doi:10.1016/S0025-3227(0200174-3

Ryan H.F. and D.W. Scholl (1989), The evolution of forearc structures along an oblique convergent margin, central Aleutian Arc, *Tectonics*, 8 (3), 497-516.

Sage F., J.-Y. Collot, C.R. Ranero (2006), Interplate patchiness and subduction-erosion mechanisms; evidence from depth-migrated seismic images at the central Ecuador convergent margin, *Geology*, 34 (12), 997-1000.

Schlueter, H.U., C. Gaedicke, H.A. Roeser, B. Schreckenberger, H. Meyer, C. Reichert, Y. Djajadihardja, A. Prexl (2002), Tectonic features of the southern Sumatra-western Java forearc of Indonesia, *Tectonics*, 21 (5), 15 pp.

Shipley T.H. and G.F. Moore (1985), Sediment accretion and subduction in the Middle America Trench, in: Formation of Active Ocean Margins, Terra Sci. Pub., Tokyo, 221-255, Eds: Nasu N. et al.

Singh S.C., H. Carton, P. Tapponnier, N.D. Hananto, A.P.S. Chauhan, D. Hartoyo, M. Bayly, S. Moeljopranoto, T. Bunting, P. Christie, H. Lubis, J. Martin (2008), Seismic evidence for broken oceanic crust in 2004 Sumatra earthquake epicentral region, Nature, doi: 10.1038/ngeo336.

Taylor B. (1992), Rifting and the volcanic-tectonic evolution of the Izu-Bonin-Mariana Arc, in: *Proc. ODP, Sci. Results*, 126: College Station, TX (Ocean Drilling Program), 627-651, Eds: Taylor B., K. Fujioka et al, doi:10.2973/odp.proc.sr.126.163.1992,.

Taylor B. and D.E. Hayes (1983), Origin and History of the South China Sea Basin, In: The Tectonic and Geologic Evolution of Southeast Asian Seas and Islands, Geophys. Monograph Ser., 27, 23-56, AGU, Washington, D.C, Eds: D.E. Hayes.

van der Werff W. (1995), Structure and morphotectonics of the accretionary prism along the Eastern Sunda-Western Banda Arc, *J. Southeast Asian Earth Sci.*, 11 (4), 309-322.

Vanneste L.E., R.D. Larter, D.K. Smythe (2002), Slice of intraoceanic arc: Insights from the first multichannel seismic reflection profile across the South Sandwich island arc, *Geology*, 30 (9), 819-822.

Vanneste L.E. and R.D. Larter (2002), Sediment subduction, subduction erosion, and strain regime in the northern South Sandwich forearc, *J. Geophys. Res.*, 107 (B7), 10.1029/2001JB000396.

von Huene R. (1986), Seismic images of modern convergent margin tectonic structure, *AAPG Studies in Geology*, 26.

von Huene R. and D. Klaeschen (1999), Opposing gradients of permanent strain in the aseismic zone and elastic strain across the seismogenic zone of the Kodiak shelf and slope, Alaska, *Tectonics*, 18 (2), 248-262.

Westbrook G.K., J.W. Ladd, P. Buhl, N. Bangs, G. Tiley (1988), Cross section of an accretionary wedge; Barbados Ridge Complex, *Geology*, 16 (7), 631-635.